Revisiting analytic shear-lag models for predicting creep in composite materials

Alexander Dyck[a], Daniel Wicht[a], Alexander Kauffmann[b], Martin Heilmaier[b], and Thomas Böhlke[a,*]

[a]Institute of Engineering Mechanics, Karlsruhe Institute of Technology (KIT), Kaiserstraße 10, 76131 Karlsruhe, Germany; {alexander.dyck, daniel.wicht, thomas.boehlke}@kit.edu
[b]Institute for Applied Materials, Karlsruhe Institute of Technology (KIT), Engelbert-Arnold-Straße 4, 76131 Karlsruhe, Germany; {alexander.kauffmann, martin.heilmaier}@kit.edu
[*]Correspondence to thomas.boehlke@kit.edu

December 5, 2022

Abstract

Abstract

Analytic shear-lag models enjoy great popularity for assessing and interpreting microstructure dependent stationary creep in fibrous metal composites, especially the formulation of Kelly-Street [Kelly and Street, Proc. Roy. Soc. A 328 (1972) 267-293]. Beyond the original model's scope, i.e. large aspect ratios of inclusions, predictions are highly inaccurate, which was recently pointed out by Wicht et al. [Wicht et al., Acta Materialia 226 (2022)], by comparing model predictions to micromechanical Fast-Fourier-Transform-based simulations. In this study we therefore modify basic Kelly-Street model assumptions, concerning effective creep rate, stress transfer and inclusion spacing to arrive at a modified model with an extended scope. To validate the modified model, we benchmark the model against Fast-Fourier-Transform-based micromechanical simulations. We show, that the proposed modifications are successful in extending the model's scope to inclusions with small aspect ratios < 20. Thus, the reformulated model is a powerful tool to describe and interpret microstructure dependent creep.

Keywords: Stationary creep, Shear-lag modeling, Micromechanical modeling, Morphology variation

A popular model for predicting and interpreting microstructure-dependent creep of fibrous and cellular metal composites is the analytic 1D shear-lag model proposed by Kelly and Street, originally published in 1972 [1, 2]. It allows the interpretation of experimental data, by linking changes in creep rates to variations in microstructure. For a given load, the model predicts stationary creep rates assuming either creeping or rigid inclusions for varying inclusion aspect ratios and volume fractions. The model owes its popularity to simplicity and straightforward implementation. Applications include creep rate predictions for lead phosphor-bronze [1], Ni-W [3], Al-SiC [4,5], niobium silicides [6], NiAl-Cr [7] and NiAl-Mo [8,9]. The model is used beyond it's scope routinely, even though several publications pointed at the limited applicability. Usually the following aspects are named limiting factors for the model's scope:

- Some inclusions have a finite creep resistance [6,10].

- The model neglects stress transfer at fiber ends [4,10,11].

- The model assumes a uniform matrix deformation rate, which is set equal to the composite's deformation rate [10, 12].

In a recent study by Wicht et al. [10], cellular NiAl-Mo is investigated, where significant deviations between creep rate predictions based on the rigid Kelly-Street model and creep rates computed by micromechanical FFT-based simulations arise. Creep rates deviate by up to an order of magnitude from numerical simulations, when small aspect ratios ≤ 20 are considered. As in previous publications, the deviation is attributed to a finite creep resistance of the inclusions and an inhomogeneous strain-rate field for low aspect ratios.

These observations demonstrate, that the application of the Kelly-Street model needs to be carefully considered, before experimental data can be interpreted. In the present study, we aim at modifying the original Kelly-Street model, to extend the model's scope to morphologies with small inclusion aspect ratios. The goal is to propose a reliable model, which accurately predicts microstructure dependent creep for a wide range of morphologies. To validate the modified model we use Fast-Fourier-Transform-based (FFT-based) micromechanical solvers, computing effective creep rates for artificially generated microstructures.
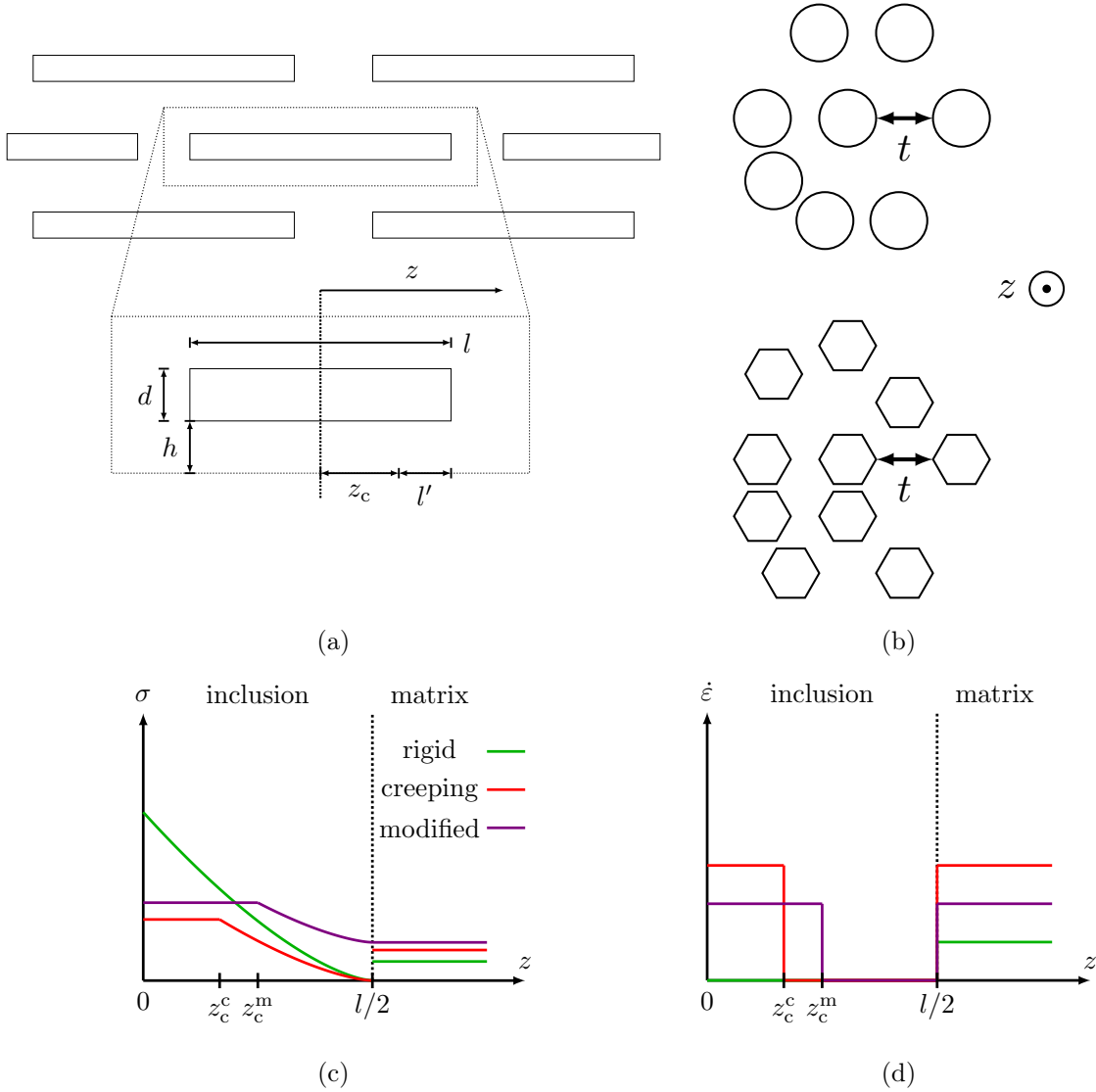
Figure 1: Schematic model diagrams for the original Kelly-Street model and and its adopted version proposed in this article. a) Considered unit cell. Load is applied in z direction. b) Cross section of unit cell perpendicular to z with circular inclusions (above), cellular inclusions (below) and average inclusion spacing $t = 2h$. c) Normal stress distribution within inclusion and matrix for the original and modified model. d) Creep rate distribution within inclusion and matrix for the original and modified model. z_c^c and z_c^m denote the rigid inclusion regions for the creeping and modified model.

The Kelly-Street model, c.f. Fig. 1 a), considers a volume element composed of a prismatic inclusion of length l and diameter d embedded in the matrix material and subjected to a uniaxial effective stress. The model approximates spacing between inclusions by a geometrical parameter h, which is specified by d and the volume fraction of the inclusions ϕ. The inclusions are assumed to behave either rigid or creeping. The transient regime of creep is neglected in the model.

The original model assumptions and equations are summarized below for the rigid and creeping inclusion models. These are

- a constant strain rate in the matrix, which is equal to the effective strain rate in the composite,

- stress transfer at inclusion ends ($z = l/2$) is neglected, c.f. Fig. 1 c),

3

- (when applicable) inclusions creep with the same rate as the matrix in the center, while a zone l' at each end is rigid, c.f. Fig. 1 d),

- (when applicable) creep behavior in both matrix and inclusion is governed by a power law and

- an estimated inclusion spacing based on hexagonal circle packing, c.f. Fig. 1 b).

The following summary of the rigid model is taken from Refs. [2, Sec. 3.1] and [6, Sec. 2.1]. Stationary creep behavior of the matrix material is assumed to follow a power law according to

$$\dot{\varepsilon}^{\mathrm{m}} = \dot{\varepsilon}_0^{\mathrm{m}} \left(\frac{\sigma^{\mathrm{m}}}{\sigma_0^{\mathrm{m}}} \right)^n , \tag{1}$$

with matrix stress σ^{m}, Exponent n, reference strain rate $\dot{\varepsilon}_0^{\mathrm{m}}$ and reference stress σ_0^{m}. The shear lag formalism assumes a shear stress distribution $\tau_{\mathrm{I}}(z)$ parallel to the matrix/inclusion interface in z, due to matrix normal stress σ^{m}. Using the balance of forces in a cylindrical coordinate system, $\tau_{\mathrm{I}}(z)$ is related to a normal stress $\sigma^{\mathrm{i}}(z)$ within the inclusion via $\sigma^{\mathrm{i}}(z) = 2\tau_{\mathrm{I}}(z)$. $\sigma^{\mathrm{i}}(z)$ is depicted in Fig. 1 c). It should be noted that stress transfer across the matrix/inclusion interface at $z = l/2$ is violated, which leads to zero normal stresses at $z = l/2$ and a subsequent jump to σ^{m}. The load-carrying capacity of the rigid inclusion is based on a mean inclusion stress $\bar{\sigma}^{\mathrm{i}}$, which is retrieved by averaging $\sigma^{\mathrm{i}}(z)$ over the inclusion length l. This results in

$$\bar{\sigma}^{\mathrm{i}}(\dot{\varepsilon}) = \left(\frac{l}{d} \right)^{(n+1)/n} \left(\frac{t}{d} \right)^{-1/n} \left(\frac{2}{3} \right)^{1/n} \left(\frac{n}{2n+1} \right) \left(\frac{n}{n+1} \right) \sigma^{\mathrm{m}}(\dot{\varepsilon}) , \tag{2}$$

where the inclusion spacing $t = 2h$ is estimated from a hexagonal packing of circular inclusion cross sections, c.f. Fig. 1 b), according to

$$\frac{t}{d} = \sqrt{\frac{2\sqrt{3}}{\pi} \phi} - 1. \tag{3}$$

The relation between applied stress σ, mean inclusion stress $\bar{\sigma}^{\mathrm{i}}$ and matrix stress σ^{m} is

$$\sigma = \phi \bar{\sigma}^{\mathrm{i}}(\dot{\varepsilon}) + (1 - \phi) \sigma^{\mathrm{m}}(\dot{\varepsilon}) . \tag{4}$$

After some algebraic manipulations of Eqs. (1 - 4), the creep rate for the composite reads

$$\dot{\varepsilon} = \dot{\varepsilon}_0^{\mathrm{m}} \left(\frac{\sigma}{\sigma_0^{\mathrm{m}} \left(\Phi(l/d)^{(n+1)/n} - 1 \right) \phi + \sigma_0^{\mathrm{m}}} \right)^n , \tag{5}$$

with the stress transfer function

$$\Phi = \left(\frac{2}{3} \right)^{1/n} \left(\frac{n}{2n+1} \right) \left(\frac{n}{n+1} \right) \left(\sqrt{\frac{\pi}{2\sqrt{3}\phi}} - 1 \right)^{-1/n} . \tag{6}$$

The creeping model assumes a center region within the inclusion, where $\dot{\varepsilon}^{\mathrm{m}} = \dot{\varepsilon}^{\mathrm{i}}$, while $\dot{\varepsilon}^{\mathrm{i}} = 0$ holds for $z \in [z_{\mathrm{c}}^{\mathrm{c}}, l/2]$, c.f. Fig 1 d). Thus interface shear stress $\tau_{\mathrm{I}}(z)$ is non-zero only for $z \in [z_{\mathrm{c}}^{\mathrm{c}}, l/2]$. This leads to a constant normal stress $\sigma^{\mathrm{i}}(z)$ for $z \in [0, z_{\mathrm{c}}^{\mathrm{c}}]$, c.f. Fig. 1 c). The formalism presented above leads to a mean inclusion stress

$$\bar{\sigma}^{\mathrm{i}}(\dot{\varepsilon}) = \left(1 - \frac{n+1}{2n+1} \frac{2l'}{l} \right) \sigma^{\mathrm{m}}(\dot{\varepsilon}) , \tag{7}$$

according to Chan [6, Sec. 2.2]. Thereby $2l'/l$ denotes the quasi-rigid inclusion fraction and is computed as

$$\frac{2l'}{l} = 2 \left(\frac{l}{d} \right)^{-1} \left(\frac{\sigma^{\mathrm{i}}(\dot{\varepsilon})}{\sigma^{\mathrm{m}}(\dot{\varepsilon})} \frac{n+1}{2n} \left(\frac{3t}{4d} \right)^{1/n} \right)^{n/(n+1)} . \tag{8}$$

4

No closed-form solution for the effective creep rate can be retrieved, but (4) can be solved numerically to determine the composite's creep rate. Here we want to point out, that for the limiting case of a fully creeping fiber, i.e. $l' = 0$, the Kelly-Street model for creeping fibers reduces to the rule of mixtures, which gives a lower bound for the effective creep rate. This limit case can be summarized as

$$\sigma = (1 - \phi)\,\sigma_0^{\mathrm{m}} \left(\frac{\dot{\varepsilon}}{\dot{\varepsilon}_0^{\mathrm{m}}} \right)^{1/n} + \phi\sigma_0^{\mathrm{i}} \left(\frac{\dot{\varepsilon}}{\dot{\varepsilon}_0^{\mathrm{i}}} \right)^{1/m}. \tag{9}$$

Again, this does not yield an explicit expression for the effective creep rate, but can be solved numerically for a given stress σ.

As pointed out, the major inconsistencies in the classical Kelly-Street model arise from (i) improper modeling of the effective strain rate, (ii) a violation of stress transfer between matrix and inclusion and (iii) a restriction to inclusions of circular cross section. The following model modifications address these issues:

1) From a micromechanical perspective the effective strain is the volume average of the local strain rate in each phase. Thus the original assumption $\dot{\varepsilon}^{\mathrm{m}} = \dot{\varepsilon}$ is inaccurate. For the modified model, we treat the solution of (4) as the matrix strain rate $\dot{\varepsilon}^{\mathrm{m}}$. As the strain rate is zero in a fraction $2l'/l$ of the inclusions and equal to $\dot{\varepsilon}^{\mathrm{m}}$ in the rest, the effective strain rate computes to

$$\dot{\varepsilon} = \left(1 - \frac{2l'}{l}\phi \right) \dot{\varepsilon}^{\mathrm{m}}, \quad \text{where } \dot{\varepsilon}^{\mathrm{m}} \text{ solves Eq. (4).} \tag{10}$$

2) We assume, that the inclusion stress $\sigma^{\mathrm{i}}(z)$ at $z = l/2$ is equal to the matrix stress σ^{m}, due to the continuity of the stress vector [4, 12, 13]. This results in a modified inclusion normal stress $\sigma^{\mathrm{i}}(z)$, which is depicted in Fig. 1 c). Following the procedure of Kelly-Street for creeping inclusions yields

$$\bar{\sigma}^{\mathrm{i}}(\dot{\varepsilon}) = \left(1 - \frac{n}{2n+1}\frac{2l'}{l} \right) \sigma^{\mathrm{i}}(\dot{\varepsilon}) + \left(\frac{n}{2n+1}\frac{2l'}{l} \right) \sigma^{\mathrm{m}}(\dot{\varepsilon}), \tag{11}$$

as an expression for the mean fiber stress. The rigid inclusion fraction is adjusted to

$$\frac{2l'}{l} = 2\left(\frac{l}{d} \right)^{-1} \left(\frac{\sigma^{\mathrm{i}}(\dot{\varepsilon}) - \sigma^{\mathrm{m}}(\dot{\varepsilon})}{\sigma^{\mathrm{m}}(\dot{\varepsilon})}\frac{n+1}{2n}\left(\frac{3t}{4d} \right)^{1/n} \right)^{n/(n+1)}. \tag{12}$$

3) Kelly and Street use the minimum fiber spacing of a hexagonal circle packing (3) as an approximation of the average inclusion distance. Thus, the range of volume fractions is naturally bounded by the maximum packing density for circles. However, for non circular inclusions, e.g. NiAl-Mo with cellular inclusions, higher volume fractions up to $\phi = 1$ are geometrically feasible. Hence, we propose to use the cell distance of a hexagonal tiling, c.f. Fig. 1 b),

$$\frac{t}{d} = \frac{\sqrt{3}}{2} \left(\phi^{-1/2} - 1 \right) \tag{13}$$

as an alternative estimate for cellular structures.

We set up two benchmarks to investigate the influence of morphology on effective creep rates, as predicted by the original and the modified Kelly-Street model. We start by investigating directionally solidified NiAl-Mo, where Mo serves as an aligned strengthening phase to the NiAl intermetallic of low creep resistance. Depending on process conditions, cellular mesostructures of regular microstructure with aligned Mo fibers embedded in degenerated regions with misaligned Mo fibers and of lower fiber volume fraction form [9]. The regular, aligned regions with volume fraction ϕ provide high creep resistance (equivalent

to inclusions in the Kelly street model), while the degenerated regions result in a lower creep resistance (equivalent to the matrix in the Kelly-Street model). The resulting composite has been studied at 900° C experimentally by Seemueller et al. [9] and numerically by Wicht et al. [10] and is considered here, due to the fact that volume fractions of up to $\phi = 100\%$ are feasible. This allows us to study the model's behavior with the modified inclusion spacing of Eq. 13. In addition, the difference in creep behavior between regular and degenerated regions over the entire range of $l/d \in [5, 40]$ is rather small, i.e. the variation in $\dot{\varepsilon}$ is less than an order of magnitude, c.f. Fig. 4 b). The second system considered is a composite of cylindrical phosphor-bronze fibers, which are embedded in a lead matrix. This composite was originally studied at room temperature by Kelly and Street [1] and will be considered here, because of the large difference in stationary creep rate of inclusion and matrix.

(a)   (b)
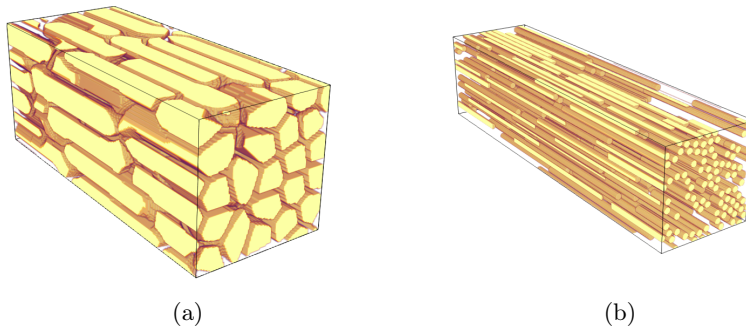
Figure 2: Synthetically generated microstructures used for micromechanical simulations: a) cellular NiAl-Mo, $\phi = 65\%$ and $l/d = 5$ (regularly aligned regions are presented as compact regions) and b) lead phosphor-bronze fibrous composite, $\phi = 30\%$ and $l/d = 25$ (fibers are depicted as compact regions).

As the individual control of the microstructure parameters ϕ as well as l/d is experimentally complicated or even impossible, we use computational homogenization to obtain effective stationary creep rates. To this end an in-house FFT-based micromechanics solver, written in Python 3.7 with Cython extensions, is used. We compute local strain and strain rate fields by solving the Lippmann-Schwinger equation [14, 15] for known constitutive laws, an explicit description of the considered microstructure and periodic boundary conditions. Using FFT-based solvers offers the flexibility to study a wide range of morphological configurations and thus to verify Kelly-Street model predictions. For our numerical simulations, we prescribe an effective uniaxial stress state in fiber direction on a volume element (VE), which is held constant until a steady-state creep rate is reached. The effective properties, i.e. the effective creep rates, are then obtained from the local fields by averaging over the volume element. The considered VEs were generated using the algorithms presented in Refs. [10] and [16]. A cellular NiAl-Mo and a lead phosphor-bronze microstructure are depicted in Fig. 2 a) and b). We note, that VE studies have been conducted to ensure a reasonable VE size. In addition, we generate five instances for each aspect ratio and volume fraction and use the mean value of effective creep rates as well as the 99% confidence interval based on the student-t distribution [17], to ensure a result independent of the individual VE. For further details concerning these FFT-based solvers and computational homogenization we refer to the recent review by Schneider [18].

The material parameters for Kelly-Street predictions and FFT simulations were taken from literature. For the Kelly-Street model, these are summarized in Tab. 1. As the creep parameters for phosphor-bronze fibers were not presented in the original manuscript, the power law parameters were obtained by a least square fitting to experimental data in Ref. [1]. We note the relatively large exponent for the fibers of 40, which is in agreement with the observations by Kelly and Street [1, Sec. 5.1] and the large difference in creep response of matrix and fiber material. A Norton plot (minimum strain rate vs. stress in double

logarithmic representation) illustrating this is depicted in Fig. 3. As Fig. 3 indicates, for large aspect ratios and inclusion volume fractions, i.e. $l/d = 100$ and $\varphi = 40\%$, the creeping and modified model both are highly accurate in predicting the stationary creep response of lead phosphor-bronze.

For the FFT-based simulations of cellular NiAl-Mo a material model developed in Ref. [10, Sec. 2.3] is used, which results in an effective uniaxial behavior equal to the power-law. In the case of lead phosphor-bronze the material behavior in FFT simulations is prescribed by a power law in both phases, where necessary parameters are chosen equal to the Kelly-Street parameters presented in Tab. 1.

Table 1: Parameters for the 1-dimensional power-law model.

Lead matrix [1]	$\dot{\varepsilon}_0^{\mathrm{m}} = 2.77 \cdot 10^{-9}\,\mathrm{s}^{-1}$	$\sigma_0^{\mathrm{m}} = 3.3\,\mathrm{MPa}$	$n = 14$
Fiber phosphor-bronze (this study)	$\dot{\varepsilon}_0^{\mathrm{i}} = 5.4 \cdot 10^{-14}\,\mathrm{s}^{-1}$	$\sigma_0^{\mathrm{i}} = 120\,\mathrm{MPa}$	$m = 40$
Matrix NiAl-Mo [10]	$\dot{\varepsilon}_0^{\mathrm{m}} = 1\,\mathrm{s}^{-1}$	$\sigma_0^{\mathrm{m}} = 503\,\mathrm{MPa}$	$n = 5.8$
Inclusion NiAl-Mo [10]	$\dot{\varepsilon}_0^{\mathrm{i}} = 1\,\mathrm{s}^{-1}$	$\sigma_0^{\mathrm{i}} = 1245\,\mathrm{MPa}$	$m = 10$
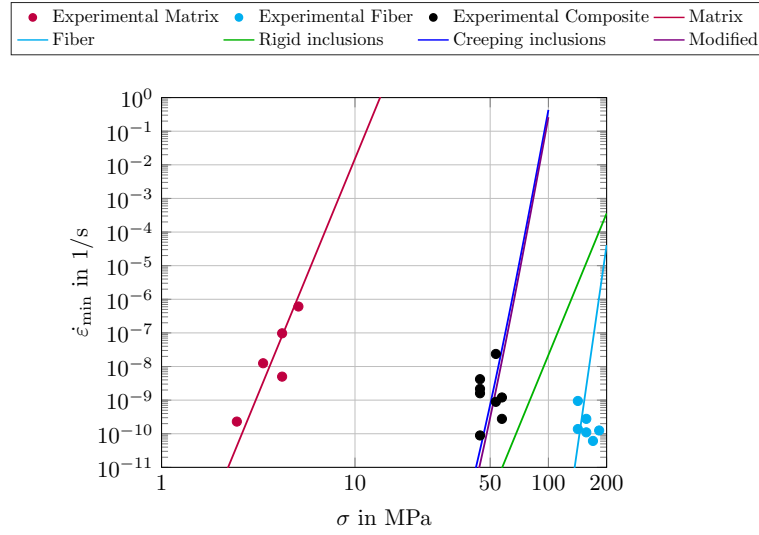
Figure 3: Norton plot of lead phosphor-bronze fiber and matrix materials measured by Kelly and Street [1], illustrating the large difference in creep resistance. In addition composite data ($l/d = 100$, $\phi = 40\%$) as well as original and modified model predictions are depicted.
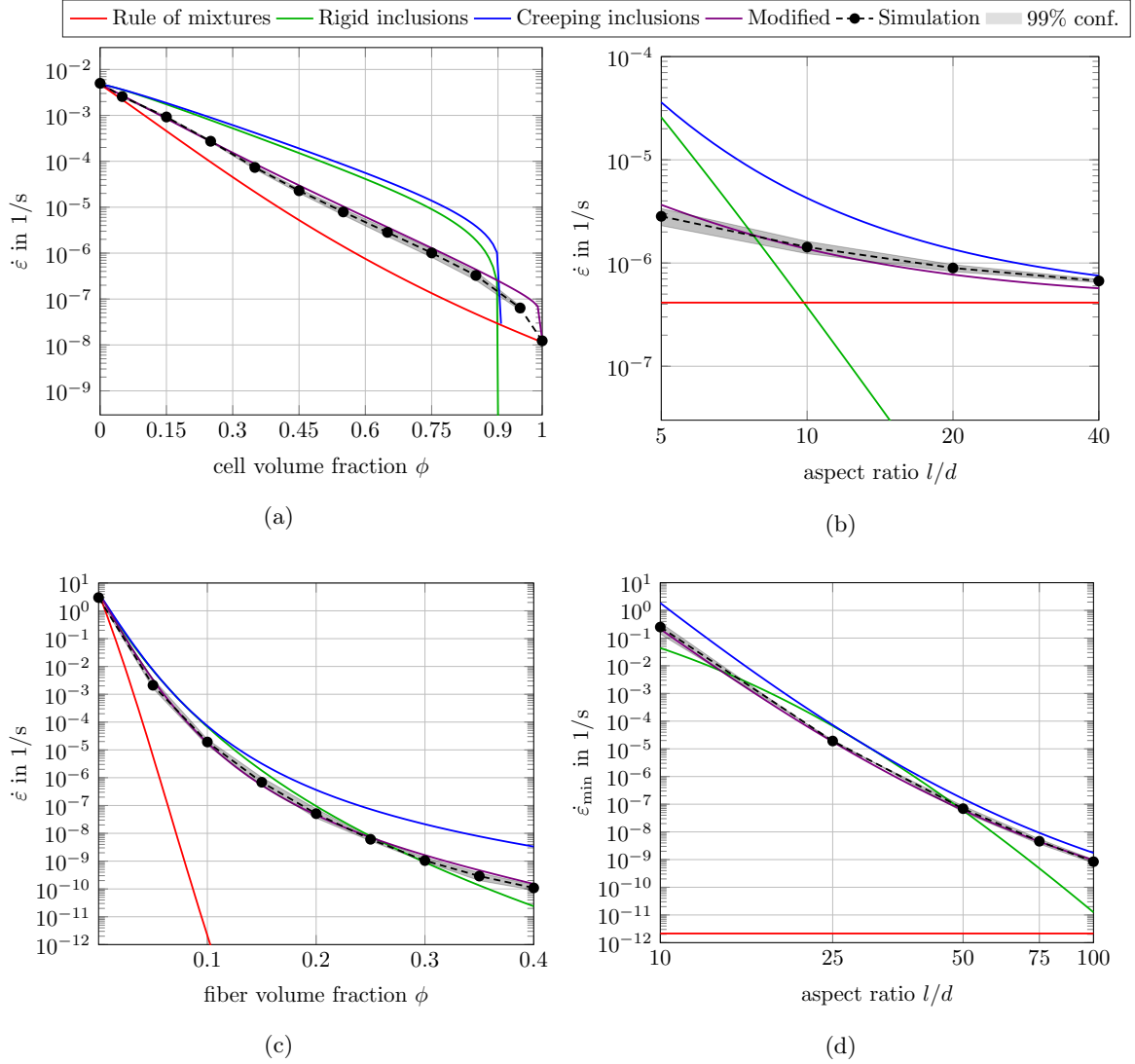
Figure 4: Kelly-Street model predictions and simulation results for cellular NiAl-Mo with $\sigma = 200\,\text{MPa}$: a) $\dot{\varepsilon}$ vs. ϕ for $l/d = 5$ and b) $\dot{\varepsilon}$ vs. l/d for $\phi = 65\%$. Kelly-Street model predictions and simulation results for lead phosphor-bronze with $\sigma = 15\,\text{MPa}$: c) $\dot{\varepsilon}$ vs. ϕ for $l/d = 25$ and d) $\dot{\varepsilon}$ vs. l/d for $\phi = 10\%$.

We start by considering cellular NiAl-Mo composite material. A comparison of simulation results to the original and modified Kelly-Street model predictions is depicted in Fig. 4 a) and b). The rule of mixtures is included to show the lower bound for the effective creep rate. Fig. 4 a) considers the full range of admissible volume fractions $\phi \in [0\,\%, 100\,\%]$ at $l/d = 5$, while Fig. 4 b) is provided for fixed $\phi = 65\%$ and varying l/d, which is the configuration studied by Seemüller et al. [9]. For computing creep rates based on the modified model we consider all modifications presented above, including the adjusted ratio of Eq. (13), to allow for cellular inclusion spacing.

The original Kelly-Street model formulations do not allow accurate descriptions of effective creep rates for small aspect ratios, c.f. Fig. 4 b), blue and green curve. This holds for the entire range of possible cell volume fractions, where the deviation is up to an order of magnitude, c.f. Fig. 4 a). Even though the inclusions are considered rigid, the Kelly-Street model underestimates the composite's creep resistance. In addition, for cell volume fractions above the maximum packing density for circles, both models degenerate. The effective creep rate, as predicted by FFT simulations, black curve, lies roughly at the

8

geometric mean of the rule of mixtures (red curve) and the original Kelly-Street models. This trend is accurately predicted by the modified model (violet curve) over the whole range of admissible volume fractions, where deviations are less than a factor of two and therefore well within the experimental scatter of minimum creep rates.

As the difference in stationary creep rate for both phases is comparably small, the effective creep rate approaches the lower bound predicted by the rule of mixtures for relatively small $l/d > 20$, c.f. Fig. 4 b). This leads to the observation, that the creeping inclusion formulation allows accurate creep rate predictions, as long as $l/d > 20$. For smaller l/d the deviations increase substantially. The modified model however captures the entire range of considered aspect ratios, closely following the FFT simulation results. The inclusions can clearly not be considered as rigid, as the rigid Kelly-Street model does not capture the trend of saturating effective creep rates for larger aspect ratios.

In the following, focus is placed on the assessment of the creep response of fibrous lead phosphor-bronze. We note, that the original fiber spacing in Eq. (3) for the modified Kelly-Street model is used, as the inclusions are circular in cross section. The results are depicted in Fig. 4 for fixed $l/d = 25$ and varying ϕ (c) and for fixed $\phi = 10\%$ for varying l/d (d).

Over the entire range of considered aspect ratios, the variation in $\dot{\varepsilon}$ is of order 10^8. Even for large aspect ratios up to 100, the results differ from the rule of mixtures by orders of magnitudes. In the range of $l/d \in [50, 100]$, the effective creep rate predictions of creeping (blue curve) and modified (violet curve) model almost coincide. Thus, both models allow an accurate prediction. However, the smaller l/d, the larger the deviations of the original model, being an order of magnitude for $l/d = 10$. Only the modified model closely follows the numerically computed creep rates for smaller aspect ratios. The rigid inclusion model (green curve) fails to capture the trend predicted by FFT simulations and is highly inaccurate for $l/d \geq 50$.

For the relatively small $l/d = 25$ in Fig. 4 c), with a varying fiber volume fraction in the range $\phi \in [0\%, 40\%]$, the large difference in creep response of the constituting phases dominates the effective composite behavior. We note, that for the whole range of ϕ, the modified and rigid models closely match the FFT-simulation results. The creeping fiber model (blue curve) is only accurate for small $\phi \leq 15\%$, but overestimates the stationary creep rate in the entire range.

To conclude this study we summarize our main results:

- When comparing the original model against FFT-based simulations, the limited scope of the original formulation is apparent.

- To extend the model's scope, we reformulated three assumptions concerning the effective strain rate, stress transfer at fiber ends and inclusion spacing.

- The benchmarks prove, that the modified model is successful in extending the model's scope, by providing exceptionally accurate predictions for morphological configurations (i.e. small fiber aspect ratios ≤ 20), where the original versions of the model remain inaccurate.

Acknowledgments

Credit author statement

Alexander Dyck and Daniel Wicht Investigation, Methodology, Software, Visualization, Writing – original draft. **Alexander Kauffmann**: Conceptualization, Visualization, Writing – review & editing. **Martin Heilmaier and Thomas Böhlke**: Conceptualization, Supervision, Resources, Funding acquisition, Writing – review & editing.

References

[1] A. Kelly and K. N. Street, "Creep of discontinuous fibre composites I. Experimental behaviour of lead-phosphor bronze," Proceedings of the Royal Society of London A, vol. 328, no. 1573, pp. 267–282, 1972.

[2] A. Kelly and K. N. Street, "Creep of discontinuous fibre composites II. Theory for the steady-state," Proceedings of the Royal Society of London A, vol. 328, no. 1573, pp. 283–293, 1972.

[3] H. Lilholt, "Creep of fibrous composite materials," Composites Science and Technology, vol. 22, no. 4, pp. 277–294, 1985.

[4] V. C. Nardone and K. M. Prewo, "On the strength of discontinuous silicon carbide reinforced aluminum composites," Scripta Metallurgica, vol. 20, no. 1, pp. 43–48, 1986.

[5] S. Goto and M. McLean, "Role of interfaces in creep of fibre-reinforced metal-matrix composites-II short fibres," Acta Metallurgica Et Materialia, vol. 39, no. 2, pp. 165–177, 1991.

[6] K. S. Chan, "Modeling creep behavior of niobium silicide in-situ composites," Materials Science and Engineering: A, vol. 337, no. 1–2, pp. 59–66, 2002.

[7] E. Bullock, M. McLean, and D. E. Miles, "Creep behaviour of a Ni-Ni$_3$Al-Cr$_3$C$_2$ eutectic composite," Acta Metallurgica, vol. 25, no. 3, pp. 333–344, 1977.

[8] L. Hu, G. Zhang, W. Hu, G. Gottstein, S. Bogner, and A. Bührig-Polaczek, "Tensile creep of directionally solidified NiAl–9Mo in situ composites," Acta Materialia, vol. 61, no. 19, pp. 7155–7165, 2013.

[9] C. Seemüller, M. Heilmaier, T. Haenschke, H. Bei, A. Dlouhý, and E. P. George, "Influence of fiber alignment on creep in directionally solidified NiAl-10Mo in-situ composites," Intermetallics, vol. 35, pp. 110–115, 2013.

[10] D. Wicht, A. Kauffmann, M. Schneider, M. Heilmaier, and T. Böhlke, "On the impact of the mesostructure on the creep response of cellular NiAl-Mo eutectics," Acta Materialia, vol. 226, p. 117626, 2022.

[11] A. F. Whitehouse, "Creep of Metal Matrix Composites," in Comprehensive Composite Materials (A. Kelly and C. Zweben, eds.), pp. 371–418, Oxford: Pergamon, 2000.

[12] M. Mondali, A. Abedian, and A. Ghavami, "A new analytical shear-lag based model for prediction of the steady state creep deformations of some short fiber composites," Materials & Design, vol. 30, no. 4, pp. 1075–1084, 2009.

[13] H. Fukuda and T. W. Chou, "An Advanced Shear-Lag Model Applicable to Discontinuous Fiber Composites," Journal of Composite Materials, vol. 15, no. 1, pp. 79–91, 1981.

[14] H. Moulinec and P. Suquet, "A fast numerical method for computing the linear and nonlinear mechanical properties of composites," Comptes Rendus de l'Académie des sciences. Série II. Mécanique, physique, chimie, astronomie, 1994.

[15] H. Moulinec and P. Suquet, "A numerical method for computing the overall response of nonlinear composites with complex microstructure," Computer methods in applied mechanics and engineering, vol. 157, no. 1-2, pp. 69–94, 1998.

[16] M. Schneider, "The sequential addition and migration method to generate representative volume elements for the homogenization of short fiber reinforced plastics," Computational Mechanics, vol. 59, no. 2, pp. 247–263, 2017.

[17] M. Schneider, M. Josien, and F. Otto, "Representative volume elements for matrix-inclusion composites-a computational study on the effects of an improper treatment of particles intersecting the boundary and the benefits of periodizing the ensemble," Journal of the Mechanics and Physics of Solids, vol. 158, p. 104652, 2022.

[18] M. Schneider, "A review of nonlinear FFT-based computational homogenization methods," Acta Mechanica, vol. 232, no. 6, pp. 2051–2100, 2021.